Robotics Research Journal
Vol. 1, No. 1; 2018
Published by CanSRG
http://cansrg.com/journals/rrj/

RTK enhanced Precision Geospatial Localization Mechanism for Outdoor SfM Photometry Applications

Dugan Um
Texas A&M University – CC, 6300 Ocean Dr. Corpus Christi, TX 78412 USA

Abstract

In this paper, we propose a UGV (Unmanned Ground Vehicle) traction mechanism and efficient motion planning means for SfM (Structure from Motion) in outdoor applications. An energy efficient traction mechanism is essential for battery driven UGVs to minimize energy cost. In addition, an autonomous path planning and motion control scheme has to be implemented for SfM especially for various outdoor applications. The photographic detailed 3D surface construction technology has potential for various applications in many fields. UAVs (Unmanned Aerial Vehicles) are dominant in 3D photometry applications with the advantage of relatively easy path planning and control in the air. An autonomous UGV based 3D photometry is, however, still a daunting task due to various and complex structures on the ground. The main challenge is to ensure obtaining a complete set of photography for a target site, minimizing duplication for less data processing and yet to have enough overlap between photos for stitching process.

The main contribution of this paper includes technical resolutions of challenging 3D surface reconstruction by a UGV in outdoor environments. Three main technical challenges have been identified: minimum energy loss by enhanced traction mechanism for wider area coverage, motion control for high quality SfM, and path planning with collision avoidance for complete 3D surface construction. In order to resolve these 3 issues, we designed a UGV with a novel traction mechanism for minimum energy loss, and developed a path control algorithm using RTK-GPS based precision mission planning.

Keywords: *SfM, modularized robot; traversability; UGV (Unmanned ground vehicle); GPS navigation.*

1. Introduction

Mobile robots are required to navigate and map unknown environments for numerous applications. Some of these applications include reconnaissance, coverage, search and rescue, and planetary missions [1]. In this paper, we propose a modularized UGV mechanism and a control scheme for outdoor SfM applications. Autonomous path planning and motion control have to be implemented for SfM especially in outdoor applications. The main challenge of outdoor SfM is to obtain a complete set of photography for a target site, minimizing duplication for less data processing and yet ensuring enough overlaps between photographs for post stitching process.

Submitted: January 17, 2018 Accepted: June 26, 2018

The main contribution of this paper includes technical resolutions of challenging 3D surface reconstruction by a UGV in outdoor environments. Three main technical challenges include motion control for high quality SfM, path planning with collision avoidance for complete 3D surface construction, and the capability of energy efficient traversability. In order to resolve these issues, the authors at TAMUCC (Texas A&M University – Corpus Christi) and Phomatix (https://www.phomatix.com) designed a UGV with the capability of path planning and navigation by RTK (Real-Time Kinematics) GPS based mission planning. In addition, we utilize the Photoscan tool on TAMUCC cloud computing HUB, which permits open access to the public by registration (http://uashub.tamucc.edu/) for SfM processing. TAMUCC UAS HUB maintains 1 node of 32 cores, 128GB memory, 30TB of storage. Photoscan cluster is composed of 8 Nodes with 4 to 16 cores, Nvidia GTX 980 GPUs and total 100 Terra bite memory storage to support up to 10 SfM parallel processing.

Autonomous UGVs are typically equipped with one or more sensors such as sonar, laser and vision, which are primarily used to create 2D and/or 3D environmental maps. Precise 3D outdoor mapping by a UGV is, however, still a daunting task. Some authors rely exclusively on a single modality of sensors for the creation of the 3D structural map. In [2], a visual SLAM (Simultaneous Localization and Mapping) approach that relies upon visual landmarks and geometric constraints in a hierarchical manner is proposed. The authors developed a hierarchical conceptual map that has various advantages such as allowing better SLAM parameter estimation, reducing the computational cost for path planning and facilitating human-to-robot interaction. Pradeep et al. [3] proposed a stereo-based visual SLAM approach that uses SIFT (scale-invariant feature transform) features to create an online multi-resolution dictionary of distinct features. This online dictionary enables loop closure without offline processing. Instead of occupancy maps, the authors built 3D reconstructions of the world, which were intended to assist the visually impaired. Zask and Dailey [4] focused on developing a textured 3D mapping model for improved search and rescue applications. In this work, the authors attempted to reduce the processing time to make it possible for real time 3D structure mapping. They used a monocular image sequence to incrementally create a 3D surface model. The authors made use of the isosurface of a coarse 3D occupancy grid in such a way that the environment can be readily visualized and explored whereas on the same hand, allow grid updates and isosurface calculation to be done quickly. Botterill et al. [5] dealt with the issue of scale drift in mono SLAM by relying upon object recognition. They developed an approach that was tested in an outdoor environment over a distance of 2.5km. The approach needs a learning process to begin with whereby the robot learns the classes of objects in an environment then estimates the distribution of sizes of objects in each class. This knowledge is then used to correct for the inherent scale drift that occurs with mono SLAM applications. Other researchers take advantage of active laser sensors which can operate in low light environments as well as directly acquire 3D coordinate data. Espino et al. [6] reported on the work done by their team CoreBots, which participated in the CAROTTE Robotics Contest. They focused on the issue of tracking the mobile robot as it explores an indoor environment. Instead of using photographic sensors, which can provide high-level semantic information, the authors here used two lasers, one for localization and mapping and the other for obstacle detection.

Autonomous outdoor 3D mapping requires a mobile platform by which environmentally significant features are captured for structural reconstruction. Although complete spatial coverage is required to guarantee the mapping completeness, navigation should assure mapping efficiency with minimum duplication among collected data. In order to solve the navigation problem to assure the efficient mapping of an unknown environment, we implemented RTK based GPS navigation and

proximity sensing for precision motion control and collision avoidance capabilities for outdoor SfM applications.

2. Traversability Cost

The design philosophy of the mobile platform is based on the modularized design to achieve enhanced performance in rough terrain traversability. In the context of our study, terrain traversability is defined as the composition of linear travel cost on rough or sloped terrain and steering cost at each waypoint. We differentiate the definition of traversability from planning completeness, or accessibility to certain region. In order to enhance the traversability, we, first, study a simplified robot-terrain interaction model to design a novel traction mechanism for a modularized platform. We use the traditional skid steering as the reference for traversability cost comparison. Eventually we review simulation results of traversability costs by both traditional skid steering and novel flexible traction mechanisms.

2.1. Wheel dynamics model

As far as the traversability is concerned, we first consider travel energy cost due to the terrain roughness. To that end, we develop a wheel-dynamics model that is simple enough to estimate cost-to-go and steering cost. We consider both upslope and downslope navigation to calculate cost-to-go and steering costs to study the total energy cost for both cases. Figure 1 depicts the upslope and downslope dynamics model of a single wheel respectively.

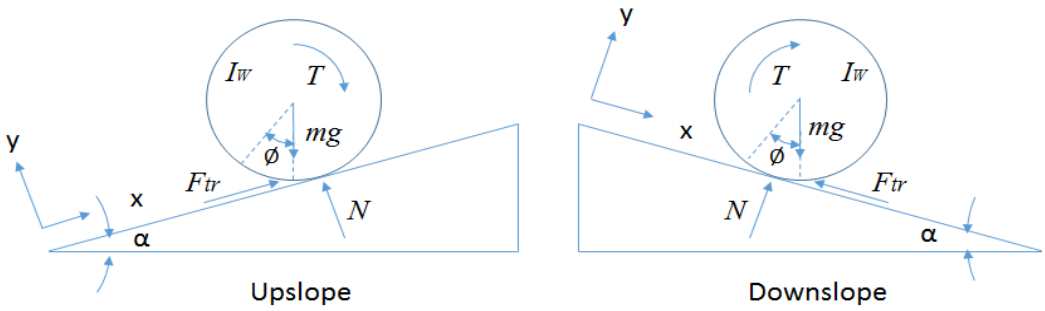

Figure 1. Wheel dynamics model.

We consider a simplified wheel-dynamics model for upslope and downslope given by

$$I_W \ddot{\emptyset}(t) = T(t) \mp r \cdot F_{tr} \quad (1)$$

$$m\ddot{x}(t) = F_{tr} - mg \cdot sin(\alpha) \quad (2)$$

where

$F_{tr} = tan(\alpha) \cdot N < \mu_s$ when no slip occurs,
$F_{tr} = \mu_d.N$ when slip occurs.

μ_s is static friction coefficient, while μ_d is dynamic friction coefficient. The static friction coefficient of '1' is widely accepted for rubber tire on concrete surface, while the value of dynamic friction coefficient for simulation is set to 0.8. The minus sign for F_{tr} in Equation (1) is for upslope, while the plus sign is for downslope. We will use the model in equation (1) to compare the traversability cost between traditional and novel traction mechanisms by simulation.

2.2. Traversability Cost

For terrain traversability cost, we develop an equation to evaluate cost by travel time along a given path. In addition, we concern about the cost required to turn at each waypoint. According to the study in **[7**], the power required to turn a skid steering mechanism is roughly twice as much as that of axial steering and it exponentially increases as the turning radius reduces. Therefore, we constitute a cost function, taking travel time and steering energy into consideration. As for the steering energy, we only consider power consumption required to turn at waypoints since the difference between skid steering and axial steering for linear motion or for large turning radius is minimal. As such, denoting $q = [x]\epsilon Q$ as the robot's state in workspace Q, and defining a path $S_q = \{q: \dot{q} = f(q,u), u\epsilon V\}$ as the evolution of $q(t)$, $t\ \epsilon Q\{t_o, t_f\}$ and control u is the set of admissible controls (we assume it constant for simple case), one dimensional linear traversability cost function associated with the total travel time and the power consumption for steering can be stated as

$$
\begin{aligned}
J(\mathrm{S}_q) &= \mathrm{k}_1 \cdot \int_{s\in \mathrm{S}_q} dt + \mathrm{k}_2 \cdot \int_{n\in \mathrm{N}_{wp}} dp_s \\
&= \mathrm{k}_1 \cdot \int_{s\in \mathrm{S}_q} \frac{1}{v(s)} ds + \mathrm{k}_2 \cdot \int_{n\in \mathrm{N}_{wp}} dp_s \\
&= \mathrm{k}_1 \cdot \textstyle\int_{s\in \mathrm{S}_q} \frac{1}{\eta(s) V_{max}} ds + \mathrm{k}_2 \cdot \int_{n\in \mathrm{N}_{wp}} dp_s
\end{aligned} \tag{3}
$$

where N_{wp} is the total number of waypoints, and p_s is the power consumed for steering. Unlike the traditional approach concerning the efficiency due to terrain condition, we rather focus more on traversability due to travel time and power for steering. The main focus of traversability study herein is on the loss in traversability cost by wheel-terrain contact condition, which in turn, will eventually lead to an optimal mechanism design that minimizes the loss. The minimum loss in traversability cost will enhance the travel distance, thus maximize energy efficiency and navigation coverage in outdoor fields for various applications.

The common energy loss on rough terrain such as farm field is due to uneven load distribution on each wheel, thus loosing tractability and eventually leading to shorter travel distance for given actuator capacity. In this paper, the context of traversability study focuses on tractability of a mobile platform on a rough terrain. Better tractability means better grasp on terrain by even mass distribution on each wheel, by which is slip or poor contact between wheel and terrain is prevented. Often observed on rough terrain navigation is that, when a wheel is lifted by terrain roughness, weight may shift to another wheel of the same row, causing increase in friction force and travel time. In this section, we study traversability cost increase on uphill and downhill conditions due to poor contact between wheels and terrain. In addition, we compare the traversability cost including steering cost later during experiments. Below is the configuration parameters for a four wheel based mobile robot platform.

Table 1. Wheel Dynamics Parameters.

Wheel radius: 0.1m
Torque: 0.5 N·m
Total weight (mg): 10 N
μ_s: 1 (between tire and concrete)

2.3. No slip condition ($\alpha < 45°$)

In order to avoid slip, first, we constrain the slope from 0 to 15°. For instance, given the torque of 0.5 N.m, depicted below are the charts of the total travel distance of a wheel with a perfect contact with the terrain during the first 30 seconds for 0° and 15° slope angle respectively.

Now, we estimate the total travel distance of a wheel when it is overloaded. Overload occurs when the other wheel of the same row loses the contact with the ground due to terrain roughness. In order to demonstrate poor or complete loss of contact case, we keep all the wheel dynamics parameters intact, except the weight of a wheel. Below we depict two charts of the total travel distance in case a wheel is overloaded due to lost contact with the ground by another wheel.

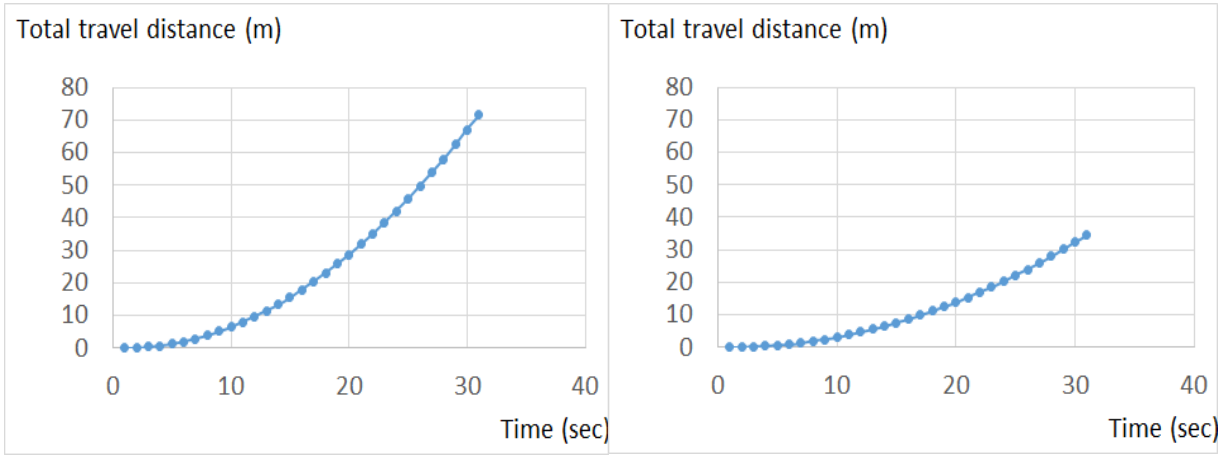

(a) 0° slope angle *(b) 15° slope angle*

Figure 2. Total travel distance (mg = 10N).

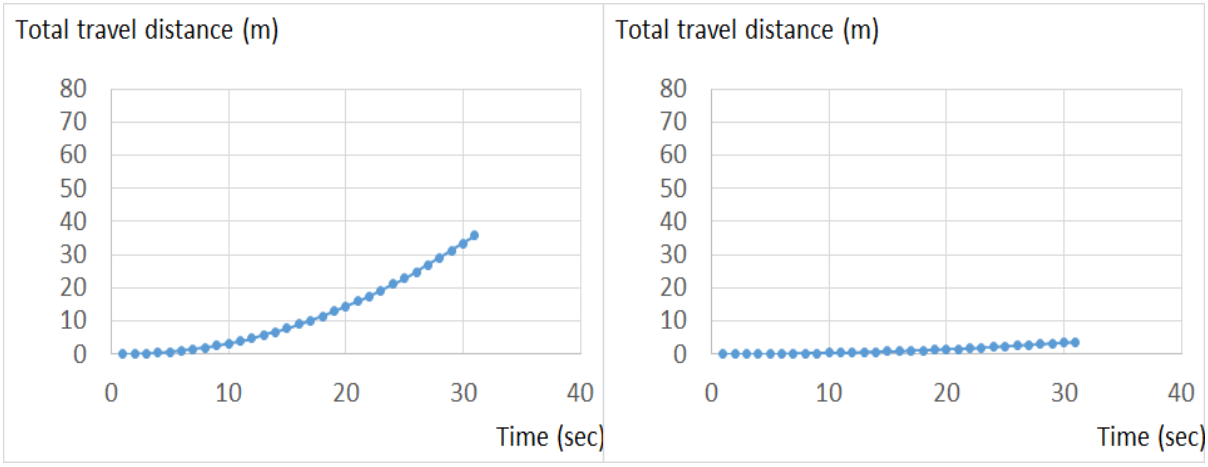

(a) 0° slope angle *(b) 15° slope angle*

Figure 3. Total travel distance (mg = 20N).

In order to compare the total travel distance between perfect contact and lost contact conditions, we investigated the travel distance ratio between perfect and poor contacts for both uphill and downhill cases, and depict them on two charts in Figure 4.

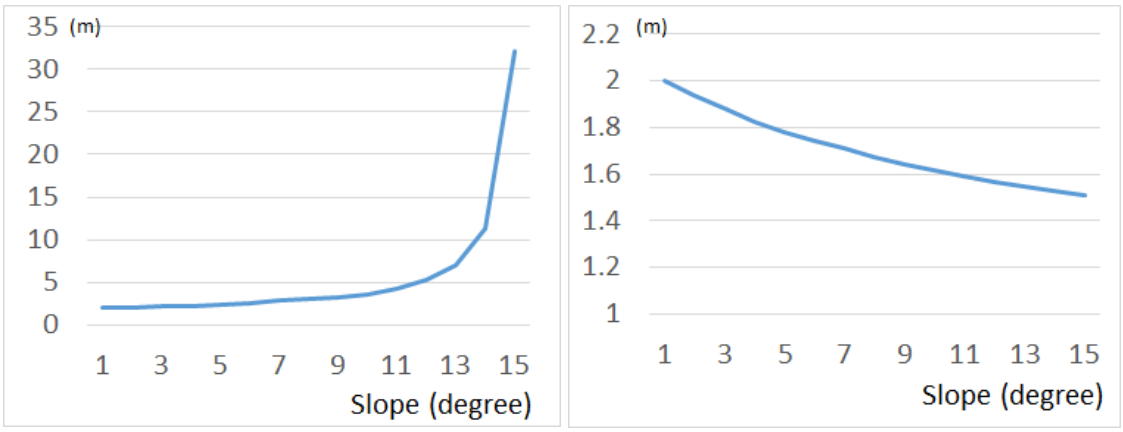

(Uphill slope) (Downhill slope)

Figure 4. Ratio of travel distance (uphill slope).

Noticeably, the contact condition influences the travel distance significantly, as the uphill slope angle becomes larger. We performed the similar study for downhill case and found that the higher slop minimizes the difference between the perfect and lost contact conditions (See Figure 4, downslope case). Evidently, however, poor contact with the ground due to terrain roughness is a significant factor in traversability of a mobile platform.

Now, by using equation (3), below we share the evaluation of the linear traversability cost function. As mentioned earlier, since the energy loss or power consumption by skid steering compared to axial steering is known already [7], we examine the time to travel cost only and verify the results of both terms in the cost function during the experiments, thus k_1 in equation (3) is equal to 1 and k_2 is set to zero for simulation. First, we assume perfect contact between all four wheels with the ground thus the weight is 10N per each wheel. As shown in Figure 5, linear traversability cost (time in seconds to reach at 10m) increases almost linearly when the wheel is in perfect contact with the terrain as the slope increases, while the traversability cost increases exponentially with poor contact.

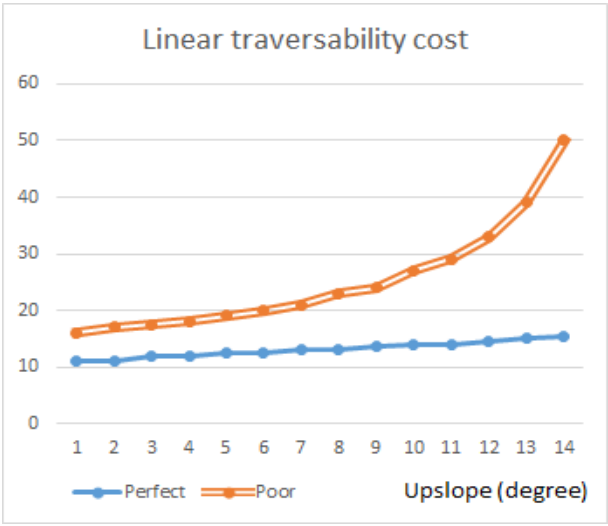

Figure 5. Linear traversability cost vs. contact condition.

The results imply that the wheel-terrain contact is of upmost importance for mobile platform traversability.

2.4. Slip condition ($\alpha > 45°$)

When a slip occurs, the second equation of wheel dynamics has to be used for traversability cost estimation. With the value of 0.8 for dynamic friction coefficient, total travel distance between perfect and poor contact conditions will be the same since the linear acceleration is not the function of mass of the wheel anymore. Therefore, the linear traversability cost will be the same as well regardless of the contact conditions. Although the tendency of poor contact may be mitigated with an appropriate suspension system, the linear traversability cost of poor contact case will be always more than that of perfect contact case. In order to assure even load distribution with perfect contact of all wheels regardless of the terrain roughness, we will introduce a novel navigation mechanism in the following section.

3. Modularized Mobile Platform

The most prevailing mobile navigation architecture is skid steering with a fixed and stout platform having little or no suspension on each wheel. Because of its simple and yet strong body dynamics, wheel or caterpillar based skid steering mechanisms have been manifested in many commercial and research grade robotic systems such as Robotnik Guardian, KIST Robhaz, or iRobot Packbot, etc [8]. Another popular mechanism is the rocker-bogie suspension that is already proven and thus employed in planetary rovers such as NASA's pathfinder, Microrover and Curiosity [9]. Many aspects of explanatory rovers have been studied from mission design and mechanism design [10][11][12] to dynamics analysis [13].

A single body, skid steering mechanism is the most compact and yet simple to operate for navigation and control. Its traversability cost, however, increases significantly on rough terrain due not only to the power consumption for steering motion, but also to poor wheel-terrain contact on rough terrain as studied in the previous section. The rocker-bogie mechanism is the most promising for rough terrain navigation ensuring maximum wheel based energy economy. However, the mechanism itself is complex, thus prone to possible failure by factors such as link friction by lubrication problem or accumulated dust on the linkage over time. Possible damage on Rocker-bogie structure by collision is also a discouraging factor. In order to minimize aforementioned problems, we propose a modularized, side rocker mechanism as illustrated in and .

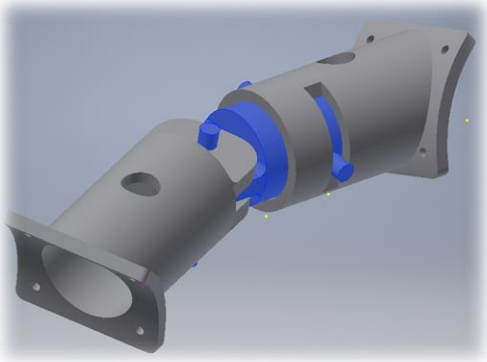

Figure 6. Flexible side-rocker mechanism.

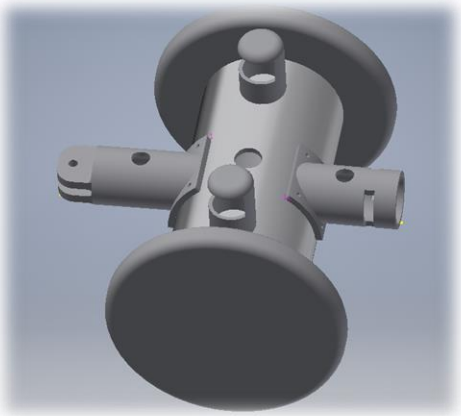

Figure 7. Modularized mobile platform.

3.1. Mechanical Design

In order to improve wheel-terrain contact, we propose a novel modularized, side rocker mechanism that enables modular design for perfect contact with terrain at all time and even distribution of load on each wheel regardless of the terrain roughness. Each module has side rocker connection compartments on the front and back sides respectively. One can use a single module with stability control in inverted pendulum configuration as well. A fully assembled two body modular robot is illustrated in . As depicted in the figure, two independent modularized bodies can be connected by the side rocker mechanism for free of side rotation and rocking motion. This will enable auto-adjustment of load distribution by gravity on each wheel, thus ensuring perfect contact between each wheel and terrain at all time.

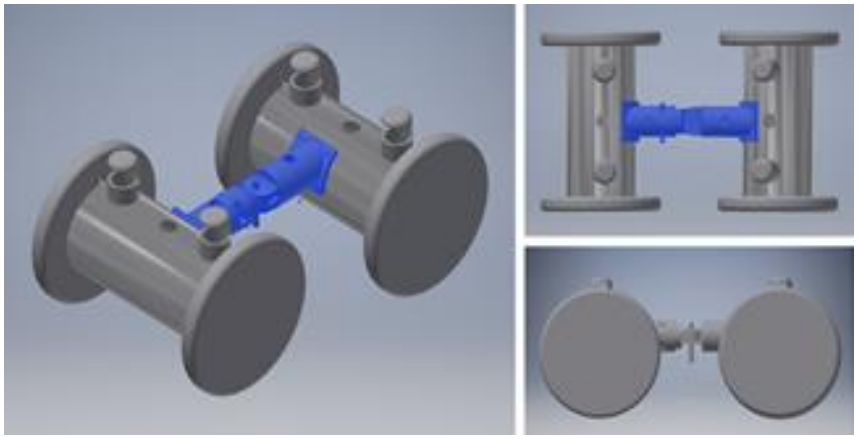

Figure 8. Combined mobile platforms.

As shown in , the side-rocker joint mechanism is designed for 30 degree side-by-side motion and 90 degree rocking motion, thus each robot body is able to adapt on rough terrains as well as to make friction free steering motion. Since each body is modular with same hardware and software, multiple bodies can be assembled for an optimal configuration with side-rocker joints. One example of centipedal configuration is depicted in Figure 10. The hollow hole in the middle of the rocker mechanism enables wire harness for coordinated motion between bodies. In addition, sensor

information can be shared to enable energy saving locomotion, which is the subject of study in the future. Given the speed command for left and right wheels, and due to the side by side joint motion, the curvature of the centipedal robot is auto-adjusted for a universal turning command that is shared by modular connections. Below, we can calculate the curvature of a centipedal robot for a given speed command for left and right wheels when the robot turns to the right.

$$r = \frac{l \cdot v_{left}}{v_{left} - v_{right}} \tag{4}$$

where r is curvature, l is distance between wheels, v_{left} is the velocity of the left wheel, while v_{right} is the velocity of the right wheel. The primary advantage of a multibody robot, however, is in its gain of travel distance since the total travel distance is proportional to the number of bodies. Therefore, one can reconfigure the robot depending on the area of coverage in various applications.

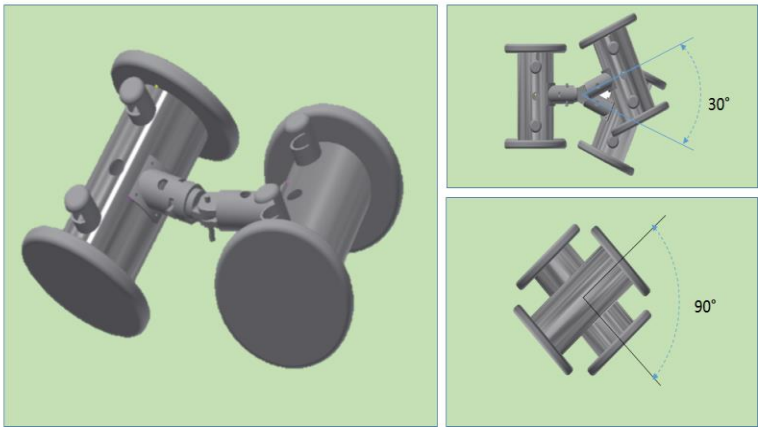

Figure 9: Flexible mobile platforms.

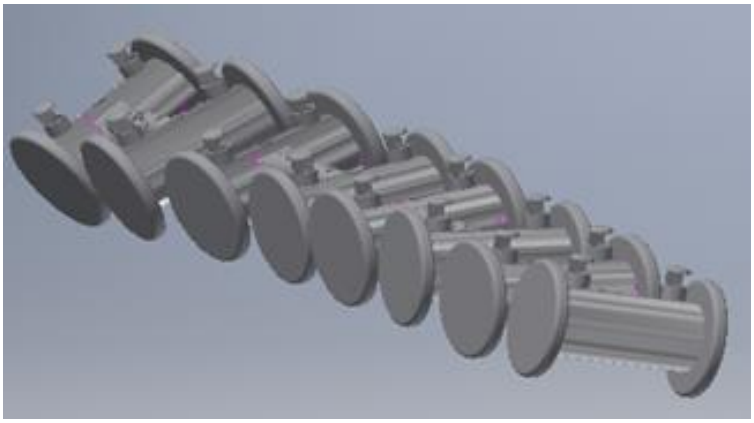

Figure 10. Mobile platforms in centipede configuration.

One thing noticed during the design stage is that the proposed flexible joint mechanism may still cause friction if all the modules are perfectly synchronized by a single motion command for steering motion (see Figure 11. (a)). In order to overcome the friction on the wheels, we implement an electric clutch to all slave modules where by no friction motion can be achieved (See Figure 11. (b), (c)).

3.2. Electrical Design

The design concept of the electrical circuit is in parallel distributed computing for maximum real-time response for all three basic functions: path planning, motion control and sensor data processing. Pixhawk embedded processor is used for GPS guided path planning, while Arduino based embedded processors are used for motion control and sensor data processing. The path planning can be done by either a human operator or by a motion planning algorithm to cover target area. Although modern path planners such as PRM [14] or RRT [15] are powerful enough to solve complex path planning tasks, we set waypoints manually due to the nature of SfM process. SfM requires parameter optimization for best quality 3D scenes.

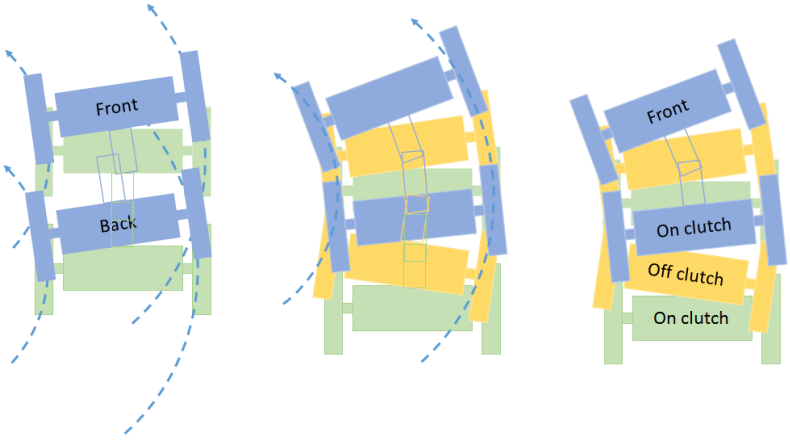

(a) Motion with friction (b) Motion with no friction (c) clutch control for no friction

Figure 11. Motion with no friction.

Motion planning algorithm for a UGV based SfM is still daunting task since it is challenging to generate a path for which all the SfM parameters are optimized [16][17][18]. For instance, following five substantive issues are what makes SfM difficult by a UGV.

1. Crowded ground environments.
2. Dynamic obstacles.
3. Stable motion for 70% overlapping.
4. Minimum duplication.
5. Complete coverage of a site.

Number 1 and 2 can be overcome by an active motion planner with collision avoidance. Number 3 and 4, however, are challenging since the robot has to understand the target 3D scene to generate optimal path. In other words, the robot requires 3D scene beforehand to generate an optimal path for SfM process. Number 5 is also challenging since the robot has to understand the target object well to generate a path for SfM process. Therefore, we currently set waypoints manually to optimize the path for SfM and the robot modifies the path to avoid collision during the navigation using scanning sonar sensors. In order to increase spatial resolution, we mount a sonar sensor unit on a servo motion controller to scan 90 degree angle with the special resolution of 10 degree (

Figure **12**). The scanning frequency is optimized to 0.3Hz for faster and yet high spatial resolution. The overall electrical system diagram is shown in Figure 13.

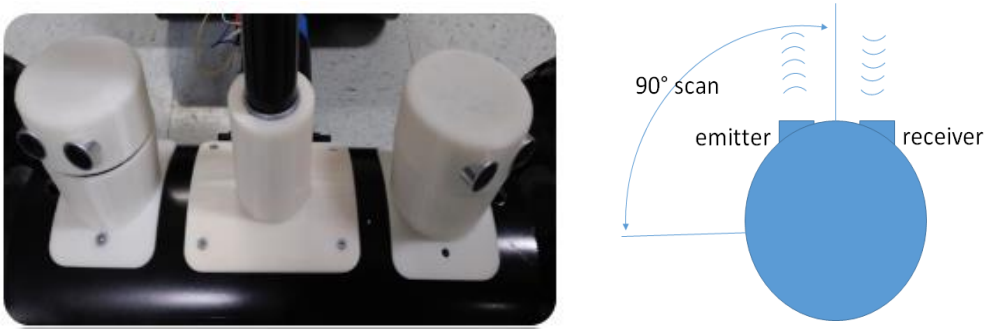

Figure 12. Servo-sonar scanner for collision avoidance.

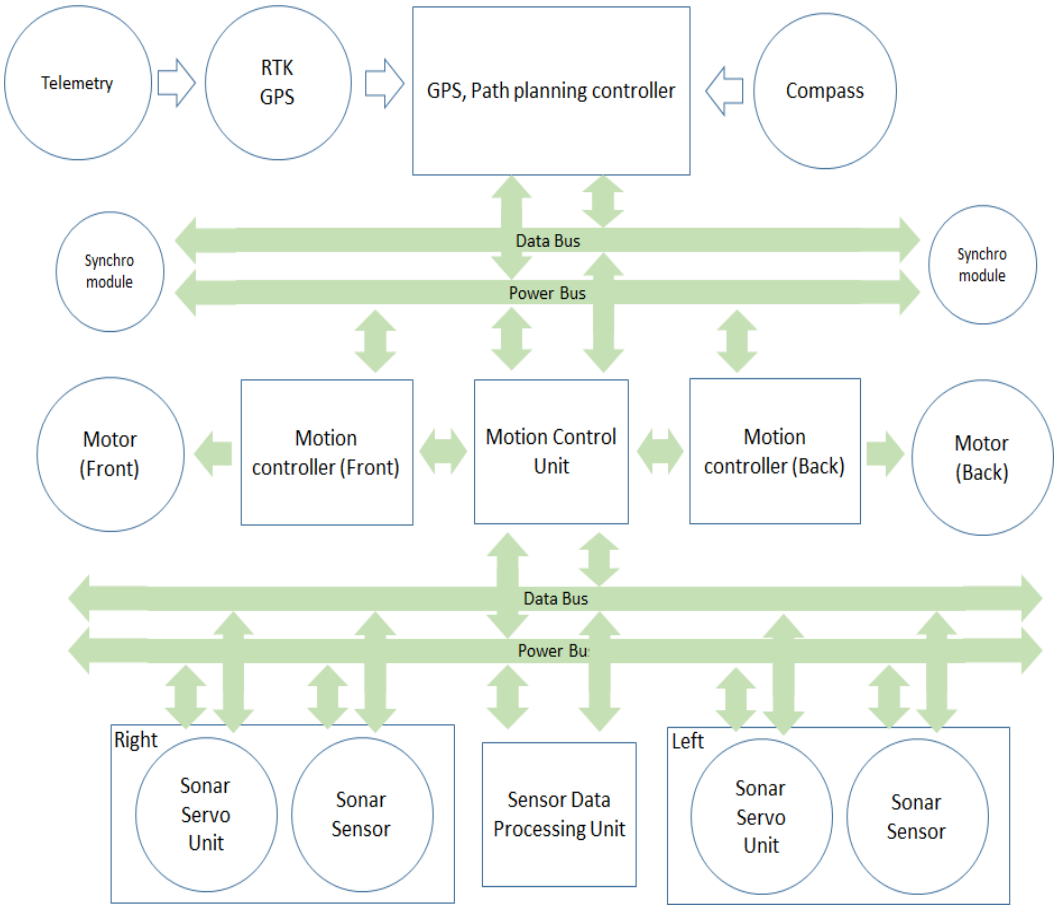

Figure 13. Electrical control diagram.

The path planning unit, once waypoints are all downloaded, starts generating paths and sends them to the motion control unit. The motion control unit, then, interprets the command and alters it if

necessary for collision avoidance. The final motion command is sent to all of the motion control units connected on the data bus via modularized connectors. Therefore, the motion control unit overrides the path planning command to avoid collision or to serve other necessary operations. In order to take advantage of the modularized design for a multiply connected system, motion synchronization by direct command sharing is proposed. A robot platform with more than two bodies may not work for a skid steer mechanism, but the proposed modular configuration enables the simple and effective modular control scheme primarily due to the flexible joint mechanism.

The experimental robot is fabricated for testing as shown in Figure 14. The modular platform developed for experiments is named TubeBot inspired by the shape of the robot. Individual TubeBot is self-contained inclusive of an embedded controller, sensors, and a battery package, thus enabling modular fabrication. However, the RTK GPS, telemetry, compass and photographic camera are installed only on the master TubeBot. For SfM photography, we use Gopro Hero 4+. In order to take photographs during the navigation, we set the shutter frequency to 2Hz.

Figure 14. Experimental setup: TubeBot.

4. Navigation Experiments

In order to generate precision waypoints and to enable precision path control, we use Real-Time Kinematics (RTK) Global Positioning System (GPS) technology for satellite error correction. GPS based robotic navigation is a popular technology for various applications such as surveillance, explosive weapon detection, chemical signature boundary detection, agriculture, and ground zero site monitoring, etc [19]. The key technology for all these applications is the Global Navigation Satellite System (GNSS), since it allows real-time positioning with global coverage and good long-term stability. To achieve required positioning accuracy at centimeter level with GNSS sensors, sophisticated GNSS algorithms such as DGPS (Differential GPS) or RTK must be used [20][21][22]. With conventional GNSS measurements, e.g. using GPS, the best positioning accuracy achievable is about 5-10m. Differential GNSS (DGNSS) and RTK are known to enhance positioning accuracy up to ‘cm’ level. To that end, augmentation data is transmitted by a wireless communication link such as cellular mobile communication or long distance telemetry devices. Taking advantage of low cost RTK GPS, we demonstrate possibility of affordable precision 3D

surface modeling by a RTK GPS enabled UGV (See Figure 15). During the test, we use a mission planner to accomplish closed loop position control and navigation to maintain ‘cm’ level accuracy.

Various waypoint radii have been tested with several configurations to find an optimal solution. Datasets from between waypoints are used to evaluate outdoor positioning accuracy of RTK-GPS enabled navigation. The overall accuracy of 30cm is achieved for linear navigation for 1km range, while 5cm is achieved for circular navigation with a diameter of 6m (Figure 16). In addition, we studied optimal settings of mission planner navigation parameters such as PID control gains, navigation speed, waypoint frequency, and waypoint angle, etc. for best 3D surface modeling results.

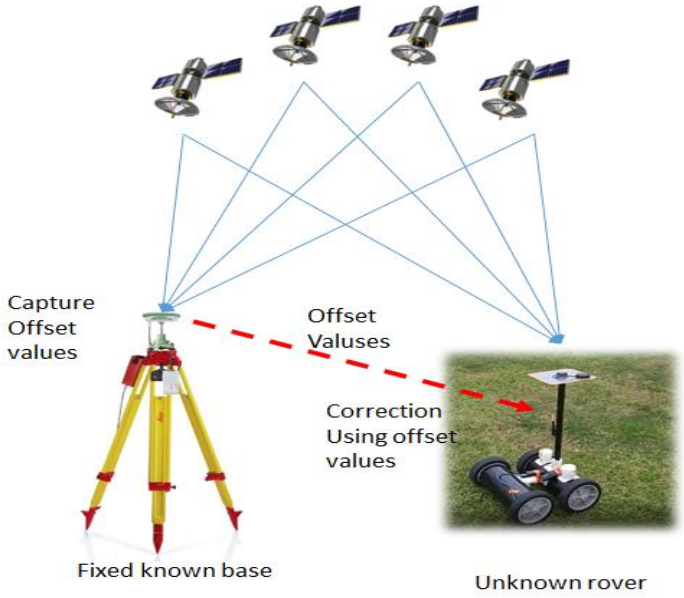

Figure 15. GNSS based precision positioning system.

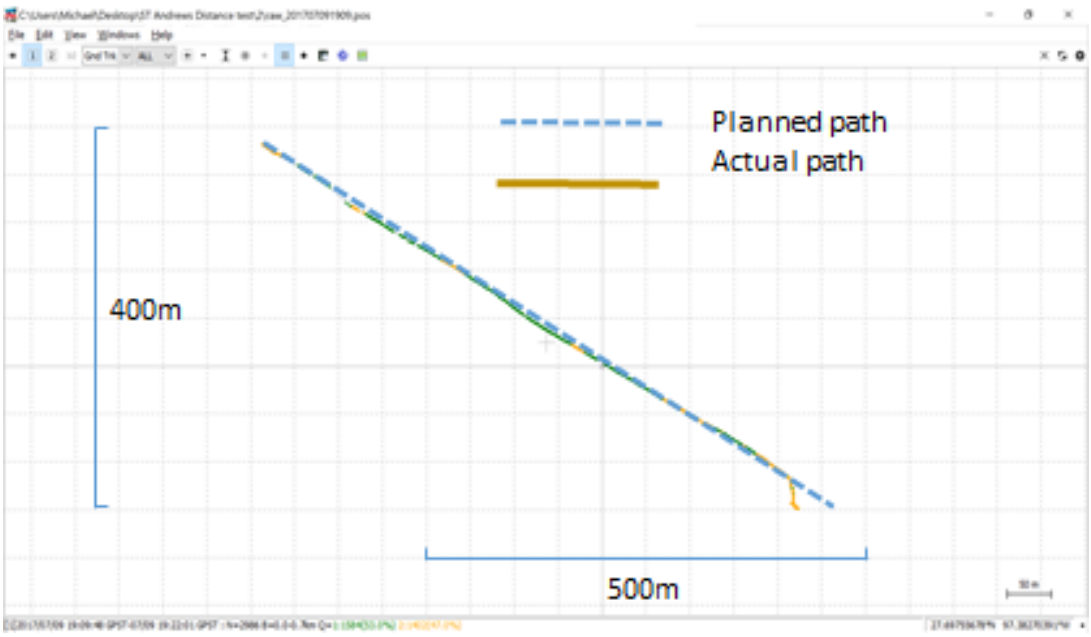

(a) Linear navigation

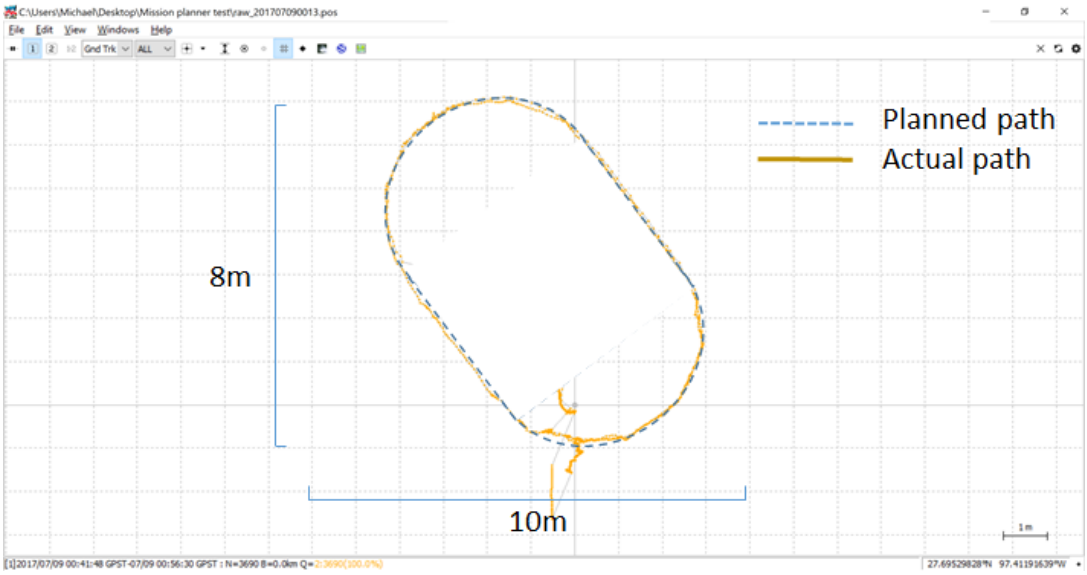

(b) Circular navigation

Figure 16. Navigation accuracy analysis.

The test bed for the assembled modularized mobile platform was the TAMUCC campus. The first test was with a single GPS without error correction for accuracy comparison. Overall accuracy by a single GPS was about 3m with the worst case error of 6.3m (Figure 17). For the second navigation test, an RTK GPS has been implemented with a fixed point GPS and a GPS on the rover for GPS error correction. The navigation result with an RTK GPS is shown in Figure 18. Overall, we achieved average accuracy of 56cm with datasets from between waypoints (Figure 19). By using photographs taken during the navigation, we generated a precision 3D surface model of outdoor campus structures with the UGV to the level unachievable by other navigation technologies (Figure 20). The corresponding surface model of the TAMUCC campus has been created from the

collected point clouds. Figure 21 illustrates the surface modeled 3D shape of the same scene on campus by point clouds. In order to make sure that the robot hits each waypoint at the given navigation speed, the waypoint error bound was set to 50cm. The overall navigation accuracy may be significantly improved by smaller error bound and slower navigation speed.

We examined the flexible side-rocker mechanism for its usefulness. Apparently, it turned out that four wheels maintained perfect contact with the terrain during the entire navigation period, resulting in minimum traversal cost for overall rough-terrain navigation. In order to evaluate traversability cost of the proposed side-rocker steering mechanism, we compared total travel distance of two different configurations: skid steering and side-rocker steering. In order to compare the total traversability cost inclusive of navigation and steering, we measure the total travel distance between skid steering and side-rocker steering with fully charged batteries. The total travel distance of the side-rocker steering with fully charged batteries is averaged to be 1.1km, which is about 50% more than that of a skid-steering (see Figure 22). The result is as is anticipated, but the discrepancy was more than expected. The skid-steering not only loses energy by side friction between wheels and the terrain, but also requires more travel cost due to poor contact between wheels and terrain. The rougher the terrain is, the more significant gain in energy saving is expected by the side-rocker steering mechanism.

Figure 17. Navigation test result with single GPS.

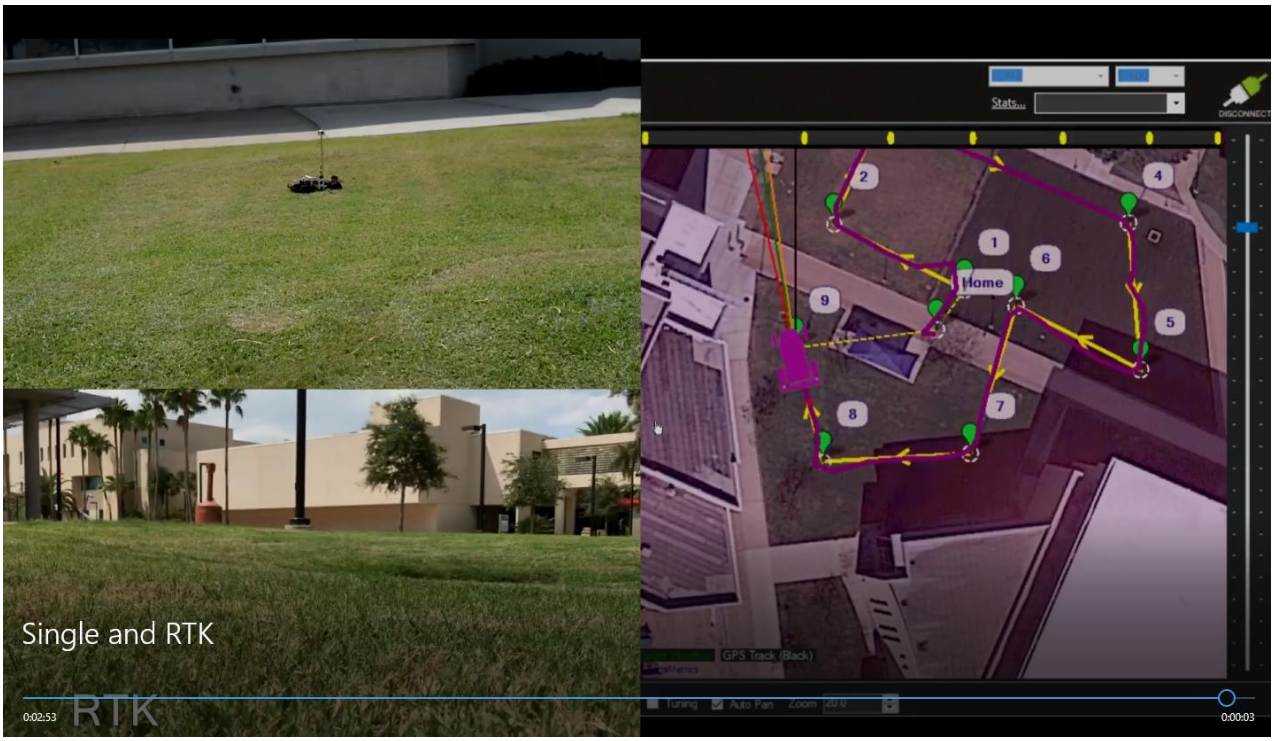

Figure 18. Navigation test result with RTK GPS.

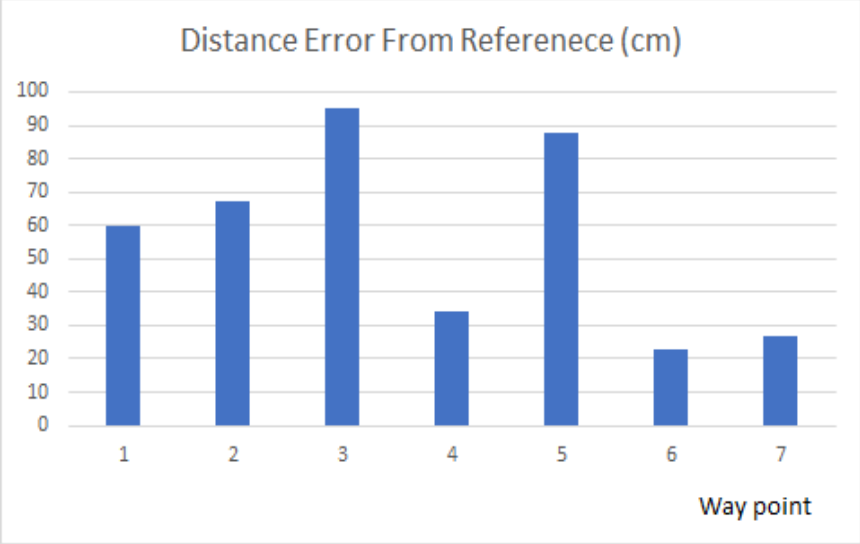

Figure 19. Navigation error estimation.

Figure 20. Campus 3D SfM model.

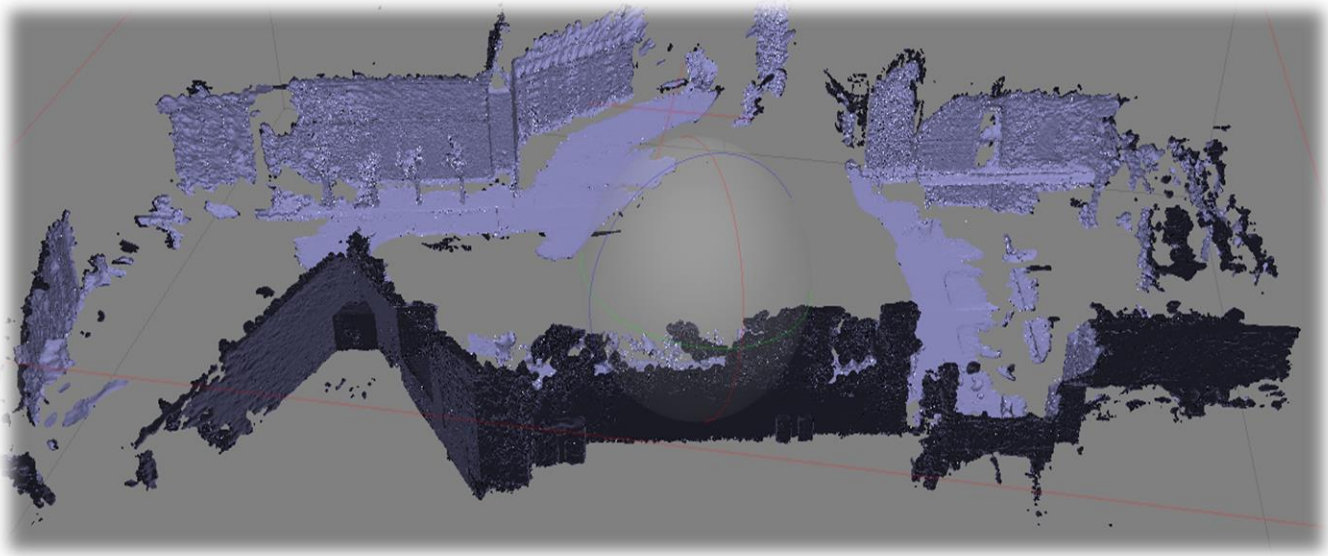

Figure 21. Campus 3D surface model.

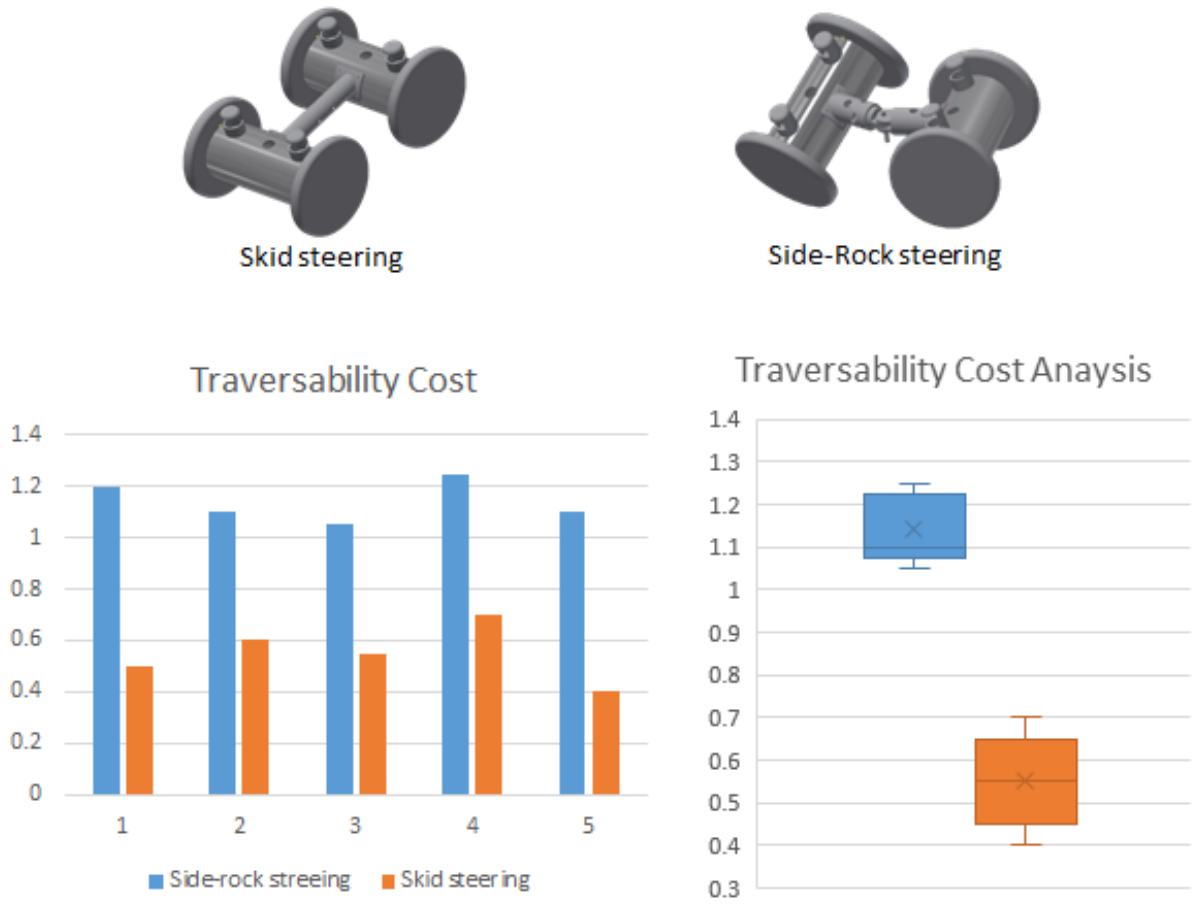

Figure 22. Traversability cost evaluation.

5. Conclusions

In this paper, we proposed a modularized UGV for energy efficient navigation for SfM in outdoor applications such as agriculture data collection, ground zero exploration, or emergency rescue operations. Three main technical challenges have been identified: minimum energy loss by enhanced traction mechanism for wider area coverage, motion control for high quality SfM, and path planning with collision avoidance for complete 3D surface construction. In order to resolve these 3 issues, we designed a modularized UGV with a side-rocker joint mechanism for minimum energy loss and the capability of path control by RTK-GPS based mission planning.

First, we studied robot-terrain interaction and terrain traversability, which led us to a modularized mobile platform with a side-rocker joint mechanism. Second, the RTK GPS based navigation has been implemented for precision outdoor positioning capability. In addition, the waypoint based autonomous navigation with collision avoidance strategy has been implemented by using a mission planner and servo-sonar sensors. Three main challenges of SfM have been identified: obtaining complete set of photography for a given site, minimizing duplication for less data processing, and yet to have enough overlaps between photos for post stitching process. In addition, situational awareness is the essential capability necessary to generate an optimal path for UGV based SfM. In order to overcome these challenges, we use manual waypoint settings, by which the mission planner controls the rover's path in 'cm' accuracy by using RTK GPS technology.

RTK GPS enabled us to achieve 30cm linear navigation accuracy for 1km range, while 5cm circular navigation accuracy for a 6m diameter track. During the outdoor navigation experiment for SfM, we achieved average accuracy of 56cm with datasets from between waypoints, and generated precision 3D surface model of outdoor structure with a proposed UGV. In order to make sure that the robot hits each waypoint at the maximum possible navigation speed, the waypoint error bound was set to 50cm. The overall navigation accuracy may be significantly improved by smaller error bound and slower navigation speed. The total travel distance with a fully charged battery is estimated to be 1.2km, which is 35% more than that of a skid-steering configuration**.** The rougher the terrain is, the more significant gain is expected. Sensor information integration for further energy saving locomotion and adaptation of the modular UGV to agricultural applications are the subject of study in the future.

References

[1] M. Rappaport, Energy-Aware Mobile Robot Exploration with Adaptive Decision Thresholds, Proceedings of ISR 2016: 47th International Symposium on Robotics, Munich, Germany, pp. 1-8, 2016.

[2] Z. Zivkovic, B. Bakker and B. Krose, Hierarchical map building using visual landmarks and geometric constraints, IEEE/RSJ International Conference on Intelligent Robots and Systems, pp. 2480-2485, 2005.

[3] V. Pradeep, G. Medioni and J. Weiland, Visual loop closing using multi-resolution SIFT grids in metric-topological SLAM, IEEE Conference on Computer Vision and Pattern Recognition, Miami, FL, pp. 1438-1445, 2009.

[4] R. Zask and M. N. Dailey, Rapid 3D visualization of indoor scenes using 3D occupancy grid isosurfaces, 6th International Conference on Electrical Engineering/ Electronics, Computer, Telecommunications and Information Technology, Pattaya, Chonburi, pp. 672-675, 2009.

[5] T. Botterill, S. Mills and R. Green, Correcting Scale Drift by Object Recognition in Single-Camera SLAM, In IEEE Transactions on Cybernetics, vol 43(6), pp. 1767-1780, 2013.

[6] J. C. Espino, B. Steux and O. E. Hamzaoui, Safe navigating system for indoor environments, The 5th International Conference on Automation, Robotics and Applications, Wellington, pp. 419-423, 2011.

[7] B. Shamah, Experimental Comparison of Skid Steering Vs. Explicit Steering for a Wheeled Mobile Robot, CMU-RI-TR-99-06, The Robotics Institute Carnegie Mellon University, Pittsburgh, Pennsylvania, March 1999.

[8] S. Kang, W Lee, M. Kim and K. Shin, ROBHAZ-Rescue : Rough-Terrain Negotiable Teleoperated Mobile Robot for Rescue Mission, Proceedings of the 2005 IEEE International Workshop on Safety, Security and Rescue Robotics Kobe, Japan, June, 2005.

[9] R. E. Arvidson, K. D. Iagnemma, M. Maimone, A. A. Fraeman, F. Zhou, M. C. Heverly, P. Bellutta, D. Rubin, N. T. Stein, J. P. Grotzinger and A. R. Vasavada, Mars Science Laboratory Curiosity Rover Megaripple Crossings up to Sol 710 in Gale Crater, Journal of Field Robotics, 23 February, 2016.

[10] P. Fiorini, Ground Mobility Systems for Planetary Exploration, Proc. 2000 IEEE Int. Conf. of Robotics and Automation, CA, USA, pp.908- 913, April, 2000.

[11] J. Aizawa, N. Yoshioka, M. Miyata and Y. Wakabayashi, Designing of Lunar Rovers for High Work Performance, Proc. i-SAIRAS'99, pp.6348, ESTEC, The Netherlands, June, 1999.

[12] Y. Kuroda, K. Kondo, K. Nakamura, Y. Kunii and T. Kubota, Low Power Mobility System for Micro Planetary Rover Micro, Proc. i-SAIRAS'99, ESTEC, The Netherlands, pp.77-82, June, 1999.

[13] K. Yoshida and H. Hamano, Motion Dynamics of a Rover with Slip-Based Traction Model, Proceedings of the 2002 IEEE International Conference on Robotics & Automation, Washington, DC, May, 2002.

[14] L. Kavraki, and J.-C. Latombe, Randomized preprocessing of configuration space for fast path planning, Proc. Int. Conf. on Robotics & Automation, pp. 2138-2145, San Diego, May, 1994.

[15] S. M. LaValle, and J. J. Kuffner, Rapidly-exploring random trees: Progress and prospects, Proc. of Workshop on the Algorithmic Foundations of Robotics, 2000.

[16] F. Steinbrucker, C. Kerl and D. Cremers, Large-scale multi-resolution: surface reconstruction from RGB-D sequences, in ICCV'13, pp. 3264–3271, 2013.

[17] D. Thomas and A. Sugimoto, A flexible scene representation for 3D reconstruction using an RGB-D camera, in Computer Vision (ICCV), 2013 IEEE International Conference on, pp. 2800–2807, Dec., 2013.

[18] C. Raposo, M. Lourenco, M. Antunes, and J. Barreto, Plane-based odometry using an RGB-D camera, in British Machine Vision Conference, 2013.

[19] C. Peijiang and J. Xuehua, Design and Implementation of Remote monitoring System based on GSM, vol 42, pp.167-175, 2008.

[20] M. Ueno and R. Santerre, GPS attitude for a berthing guidance system, Can. Aeronaut. Space J., vol 45(3), pp. 264-269, 1999.

[21] M. Ueno and R. Santerre, A combined method for GPS ambiguity resolution with single-frequency receivers: Application for ship berthing, Navigation, vol 47(2), pp. 100-111, 2000.

[22] L. P. Fortes, G. Lachapelle, M. E. Cannon, G. Marceau, S. Ryan, S. Wee, and J. Raquet, Testing of a multi-reference GPS station network for precise 3D positioning in the St. Lawrence Seaway, in Proc. Int. Tech. Meeting Satellite Div., pp. 1259-1270, Nashville, TN, 1999.

Biographical Information

Dugan Um achieved his Ph.D in Mechanical Engineering in the University of Wisconsin at Madison. Sensitive robotic skin for unknown environments motion planning was the subject of his dissertation. After he received his degree, he joined Caterpillar Inc. as a research engineer and worked for about 4 years at Caterpillar R&D group and Research center. Currently he is at Texas A&M University, Corpus Christi delivering his multiple years of engineering experiences into classes. He is serving the NSF S-STEM directorate as a board committee, securing over 2M research and educational funds at national and international level during the last 15 years of research and education in academia. His research areas include robotic motion planning, 3D sensing, UAV control, and MEMS technology. He is currently an associate professor of Mechanical Engineering, Texas A&M University-Corpus Christi.